only slightly younger ages, for example, and illustrate the pressing need for better statistics[12].

The Space Infrared Telescope Facility (SIRTF) to be launched by NASA in 2002 will go much deeper than IRAS and ISO, and will provide hundreds of new targets for further study. Improved molecular-line observations will also become possible with the high-resolution mid-infrared spectrometers nearing completion for use on large ground-based telescopes (for the 17-μm S(1) line) and the Stratospheric Observatory for Infrared Astronomy (SOFIA) (for all H_2 lines including the 28-μm S(0) transition).These diffraction-limited spectrometers will possess both the spatial and spectral resolution required to examine whether the gas and dust are co-spatial in the disks, and can establish whether the gas persists to within a few AU of the central star without the use of coronographic techniques. In the longer term, a mid-infrared spectrometer on the Next Generation Space Telescope (NGST) would make possible the detection of Earth-masses of H_2 gas at temperatures down to 50 K. By combining continuum and line studies of disks around stars up to several tens of Myr in age, it will be possible to determine both gas/dust dissipation and jovian planet formation timescales; and to examine the role of collisional, radiative and gaseous processes in shaping the evolution and survival of dust clouds in planetary systems. □

Received 25 September 2000; accepted 16 November 2000.

1. Beckwith, S. W. V. & Sargent, A. I. Circumstellar disks and the search for neighbouring planetary systems. *Nature* **383,** 139–144 (1996).
2. Aumann, H. *et al.* Discovery of a shell around Alpha Lyrae. *Astrophys. J.* **278,** L23–L27 (1984).
3. Backman, D. E. & Paresce, F. in *Protostars & Planets III* (eds Levy, E. H. & Lunine, J. I.) 1253–1304 (Univ. Arizona Press, Tucson, 1993).
4. Habing, H. J. *et al.* Disappearance of stellar debris disks around main-sequence stars after 400 million years. *Nature* **401,** 456–458 (1999).
5. Lagrange, A. M., Backman, D. E. & Artymowicz, P. in *Protostars & Planets IV* (eds Mannings, V., Boss, A. & Russell, S.) 639–672 (Univ. Arizona Press, Tucson, 2000).
6. Greaves, J. S., Coulson, I. M. & Holland, W. S. No molecular gas around nearby solar-type stars. *Mon. Not. R. Astron. Soc.* **312,** L1–L3 (2000).
7. Zuckerman, B., Forveille, T. & Kastner, J. H. Inhibition of giant planet formation by rapid gas depletion around young stars. *Nature* **373,** 494–496 (1995).
8. Dent, W. R. F., Greaves, J. S., Mannings, V., Coulson, I. M. & Walther, D. M. A search for molecular gas components in prototypical Vega-excess systems. *Mon. Not. R. Astron. Soc.* **277,** L25–L29 (1995).
9. Hildebrand, R. H. The determination of cloud masses and dust characteristics from submillimeter thermal emission. *Q. J. R. Astron. Soc.* **24,** 267–282 (1983).
10. de Graauw, T. *et al.* Observing with the ISO Short Wavelength Spectrometer. *Astron. Astrophys.* **315,** L49–L54 (1996).
11. Kessler, M. *et al.* The Infrared Space Observatory (ISO) mission. *Astron. Astrophys.* **315,** L64–L70 (1996).
12. Thi, W. F. *et al.* H_2 and CO emission from disks around T Tauri, Herbig Ae and Vega-type stars: cold and warm circumstellar gas. *Astrophys. J.* (submitted).
13. Thi, W. F., van Dishoeck, E. F., Blake, G. A., van Zadelhoff, G. J. & Hogerheijde, M. R. Detection of H_2 pure rotational line emission from the GG Tau circumbinary disk. *Astrophys. J.* **521,** L63–L66 (1999).
14. Valentijn, E. A. & Thi, W. F. ISO's Short Wavelength Spectrometer—Ultimate sensitivity. Reducing the effects of cosmic weather. *Exp. Astron.* **10,** 215–225 (2000).
15. Walker, H. J. & Heinrichsen, I. ISOPHOT observations of dust disks around main-sequence (Vega-like) stars. *Icarus* **143,** 147–154 (2000).
16. Kamp, I. & Bertoldi, F. CO in the circumstellar disks of Vega and β Pictoris. *Astron. Astrophys.* **353,** 276–286 (2000).
17. Sandford, S. A. & Allamandola, L. J. H_2 in interstellar and extragalactic ices—Infrared characteristics, ultraviolet production, and implications. *Astrophys. J.* **409,** L65–L68 (1993).
18. Hollenbach, D. J., Yorke, H. W. & Johnstone, D. in *Protostars & Planets IV* (eds Mannings, V., Boss, A. & Russell, S.) 401–428 (Univ. Arizona Press, Tucson, 2000).
19. Lagrange, A. M. *et al.* The β Pic circumstellar disk. XXIV. Clues to the origin of the stable gas. *Astron. Astrophys.* **310,** 1091–1108 (1998).
20. Heap, S. R. *et al.* STIS coronographic observations of β Pictoris. *Astrophys. J.* **539,** 435–444 (2000).
21. Klahr, H. H. & Lin, D. N. C. Dust distribution in gas disks. A model for the ring around HR 4796A. *Astron. J.* (in the press).
22. Weidenschilling, S. J. Aerodynamics of solid bodies in the solar nebula. *Mon. Not. R. Astron. Soc.* **180,** 57–70 (1977).
23. Artymowicz, P. & Clampin, M. Dust around main sequence stars: Nature or nurture by the interstellar medium? *Astrophys. J.* **490,** 863–878 (1997).
24. Barrado y Navascués, D., Stauffer, J. R., Song, I. & Caillault, J. P. The age of β Pictoris. *Astrophys. J.* **520,** L123–L126 (1999).
25. Siess, L., Forestini, M. & Bertout, C. Physics of accretion onto young stars. III. Comparisons with observations. *Astron. Astrophys.* **342,** 480–491 (1999).
26. Dunkin, S. K., Barlow, M. J. & Ryan, S. G. High-resolution spectroscopy of Vega-like stars—II. Age indicators, activity and circumstellar gas. *Mon. Not. R. Astron. Soc.* **290,** 165–185 (1997).
27. Zuckerman, B. & Webb, R. A. Identification of a nearby stellar association with the *Hipparcos* catalog: Implications for recent, local star formation. *Astrophys. J.* **535,** 959–964 (2000).
28. Jourdain de Muizon, M., Laureijs, R. J., Dominik, C. & Habing, H. J. A very cold disk of dust around the G2V star HD 207129. *Astron. Astrophys.* **350,** 875–882 (1999).
29. Fajardo-Acosta, S. B., Stencel, R. E., Backman, D. E. & Thakur, N. Infrared Space Observatory photometric search of main-sequence stars for Vega-type Systems. *Astrophys. J.* **520,** 215–222 (1999).

Acknowledgements

This work was supported by The Netherlands Organization for Scientific Research (NWO). Additional support to G.A.B. from the NASA Infrared Space Observatory (ISO), Exobiology, and Origins of Solar Systems programmes is gratefully acknowledged. A.N. is supported in part by an Agenzia Spaziale Italiana (ASI) grant. This work is based on observations with ISO, a European Space Agency (ESA) project with instruments funded by ESA Member States (especially the Principal Investigator countries: France, Germany, the Netherlands, and the United Kingdom) and with the participation of the Institute of Space and Astronautical Sciences (ISAS) and the National Aeronautics and Space Administration (NASA).

Correspondence should be addressed to G.A.B. (e-mail: gab@gps.caltech.edu).

Many-particle entanglement with Bose–Einstein condensates

A. Sørensen*, L.-M. Duan†, J. I. Cirac† & P. Zoller†

* *Institute of Physics and Astronomy, University of Aarhus, DK-8000 Århus C, Denmark*
† *Institute for Theoretical Physics, University of Innsbruck, A-6020 Innsbruck, Austria*

The possibility of creating and manipulating entangled states of systems of many particles is of significant interest for quantum information processing; such a capability could lead to new applications that rely on the basic principles of quantum mechanics[1]. So far, up to four atoms have been entangled in a controlled way[2,3]. A crucial requirement for the production of entangled states is that they can be considered pure at the single-particle level. Bose–Einstein condensates[4–6] fulfil this requirement; hence it is natural to investigate whether they can also be used in some applications of quantum information. Here we propose a method to achieve substantial entanglement of a large number of atoms in a Bose–Einstein condensate. A single resonant laser pulse is applied to all the atoms in the condensate, which is then allowed to evolve freely; in this latter stage, collisional interactions produce entanglement between the atoms. The technique should be realizable with present technology.

Consider a set of N two-level atoms confined by some external trap. In order to describe the internal properties of these atoms, it is convenient to let the internal states $|a\rangle_n$ and $|b\rangle_n$ of the nth atom represent the two states of a fictitious spin-1/2 particle with angular momentum operators $j_z^{(n)} = 1/2(|a\rangle\langle a|_n - |b\rangle\langle b|_n)$, $j_x^{(n)} = 1/2(|b\rangle\langle a|_n + |a\rangle\langle b|_n)$, and $j_y^{(n)} = i/2(|b\rangle\langle a|_n - |a\rangle\langle b|_n)$. We consider collective effects of the atoms that are described by total angular momentum operators, $\mathbf{J} = \Sigma_{n=1}^{N}\mathbf{j}^{(n)}$. The entanglement properties of the atoms can be expressed in terms of the variances and expectation values of these operators. In the Methods section we show that if

$$\xi^2 \equiv \frac{N(\Delta J_{\mathbf{n}_1})^2}{\langle J_{\mathbf{n}_2}\rangle^2 + \langle J_{\mathbf{n}_3}\rangle^2} < 1 \qquad (1)$$

where $J_{\mathbf{n}} \equiv \mathbf{n}\cdot\mathbf{J}$ and the $\mathbf{n}$s are mutually orthogonal unit vectors, then the state of the atoms is non-separable (that is, entangled). The parameter ξ^2 thus characterizes the atomic entanglement, and states with $\xi^2 < 1$ are often referred to as "spin squeezed states"[7]. Here we show how to reduce ξ^2 by several orders of magnitude using the collisional interactions between atoms in a Bose–Einstein condensate.

We consider a two-component weakly interacting Bose–Einstein condensate, which has been produced in several laboratories[8,9], and we assume that the interactions do not change the internal state of the atoms. This situation is described by the second quantized hamiltonian

$$H = \sum_{j=a,b} \int \mathrm{d}^3 r \hat{\Psi}_j^\dagger(\mathbf{r}) H_{0j} \hat{\Psi}_j(\mathbf{r}) + \frac{1}{2} \sum_{j=a,b} U_{jj} \int \mathrm{d}^3 r \hat{\Psi}_j^\dagger(\mathbf{r}) \hat{\Psi}_j^\dagger(\mathbf{r}) \hat{\Psi}_j(\mathbf{r}) \hat{\Psi}_j(\mathbf{r})$$

$$+ U_{ab} \int \mathrm{d}^3 r \hat{\Psi}_a^\dagger(\mathbf{r}) \hat{\Psi}_b^\dagger(\mathbf{r}) \hat{\Psi}_a(\mathbf{r}) \hat{\Psi}_b(\mathbf{r}) \qquad (2)$$

where $H_{0,j}$ is the one-particle hamiltonian for atoms in state j including the kinetic energy and the external trapping potential $V_j(\mathbf{r})$, $\hat{\Psi}_j(\mathbf{r})$ is the field operator for atoms in the state j, $U_{jk} = 4\pi\hbar^2 a_{jk}/m$ is the strength of the interaction between particles of type j and k, parametrized by the scattering length a_{jk}, and m is the atomic mass.

Assume that we start with a Bose–Einstein condensate in state $|a\rangle$ at very low temperature ($T \approx 0$), so that all the atoms are in a single-particle (motional) state $|\phi_0\rangle$. A fast $\pi/2$ pulse between the states $|a\rangle$ and $|b\rangle$ prepares the atoms in the state $|\phi_0\rangle^{\otimes N} \otimes (|a\rangle + |b\rangle)^{\otimes N}/2^{N/2}$ which is an eigenstate of the J_x operator with eigenvalue $N/2$. If we choose in equation (1) $\mathbf{n}_1 = [0, \cos(\theta), \sin(\theta)]$ and $\mathbf{n}_2$ along the x axis of the fictitious angular momentum, we have $\xi_\theta^2 = 1$ at $t = 0$. By using the equations of motion of the angular momentum operators in the Heisenberg picture, we find the time derivative of ξ_θ^2 at $t = 0$:

$$\frac{\mathrm{d}}{\mathrm{d}t} \xi_\theta^2 = \sin(2\theta) \frac{(N-1)(U_{aa} + U_{bb} - 2U_{ab})}{2\hbar} \int \mathrm{d}^3 r |\phi_0|^4 \qquad (3)$$

This equation shows that spin squeezing will be produced for certain angles θ if $U_{aa} + U_{bb} \neq 2U_{ab}$, as it is in the sodium experiments[9].

To quantify the amount of squeezing which may be obtained, we assume identical trapping potentials $V_a(\mathbf{r}) = V_b(\mathbf{r})$ and identical coupling constants for interaction between atoms in the same internal state $a_{aa} = a_{bb} > a_{ab}$. Physically, this could correspond to the $|F = 1, M_F = \pm 1\rangle$ hyperfine states of Na trapped in an optical dipole trap (F and M_F are the quantum numbers of the atomic angular momentum). Owing to the symmetry of these states, their scattering lengths and trapping potentials will be identical; moreover, angular-momentum conservation ensures there are no spin-exchanging collisions between these states as required by our model. This is exactly the experimental set-up used in ref. 9. In this experiment it is shown that these states have an antiferromagnetic interaction $a_{ab} < a_{aa}$ which, according to equation (3), enables the production of squeezed states. To avoid spin-changing collisions that populate the state $|M_F = 0\rangle$ (ref. 10), it is necessary to modify slightly such an experimental set-up. If the $F = 1$ manifold is coupled to the $F = 2$ with a far off-resonant blue-detuned π-polarized microwave field, the $|F = 1, M_F = 0\rangle$ state is raised in energy with respect to the $|F = 1, M_F = \pm 1\rangle$ states, because the coupling coefficient for the $|F = 1, M_F = 0\rangle \rightarrow |F = 2, M_F = 0\rangle$ transition is larger than the coefficients for the $|F = 1, M_F = \pm 1\rangle \rightarrow |F = 2, M_F = \pm 1\rangle$ transitions, and spin-exchanging collisions become energetically forbidden. If, for instance, we choose a detuning $\delta = (2\pi)25$ MHz and a resonant Rabi frequency for the $1 \rightarrow 1$ transition of $\Omega = (2\pi)2$ MHz, the energy separation is $\Delta E = 640$ nK. With a typical chemical potential $\mu \approx 220$ nK (ref. 10), this energy separation is much higher than the available energy in the collisions and the $|F = 1, M = 0\rangle$ state is completely decoupled. In ref. 10 a much smaller energy difference is shown to exclude spin-exchanging collision, and we therefore expect that much weaker fields will suffice.

The assumption $a_{aa} = a_{bb}$ has several advantages. First, it reduces the effects of fluctuations in the total particle number. If $a_{aa} \neq a_{bb}$, the mean spin performs an N-dependent rotation around the z-axis, and fluctuations in the number of particles introduces an uncertainty in the direction of the spin that effectively reduces the average value and introduces noise into the system. With $a_{aa} = a_{bb}$, the mean spin remains in the x-direction, independent of the number of atoms in the trap. Second, this condition ensures a large spatial overlap of different components of the wavefunction. After the $\pi/2$ pulse, the spatial wavefunction is no longer in the equilibrium state. That is, owing to the atomic repulsions (which are now different from before because the atoms are in different internal states), the spatial distribution of the atomic cloud will start oscillating. Furthermore, as the state of the system is now distributed over a range of number of particles in the $|a\rangle$ state (N_a), and because this number enters into the time evolution, the N_a-dependent wavefunctions ϕ_a and ϕ_b are different for particles in the states $|a\rangle$ and $|b\rangle$. With $a_{aa} = a_{bb}$, ϕ_a and ϕ_b are identical if N_a equals the average number $N/2$. In the limit of large N, the width of the distribution on different N_as is much smaller than N_a and all the spatial wavefunctions are approximately identical: $\phi_a(N_a, t) \approx \phi_b(N_a, t) \approx \phi_0(t)$. This relation is only true if $a_{aa} > a_{ab}$ where small deviations from

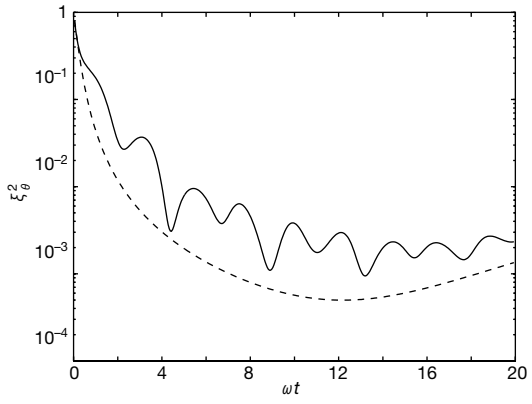

Figure 1 Reduction in the squeezing parameter ξ^2. A fast $\pi/2$ pulse between two internal states is applied to all atoms in the condensate. The subsequent free evolution with time results in a strong squeezing of the total spin. The angle θ is chosen such that ξ_θ^2 is minimal. The solid line shows the results of a numerical integration (see text). For numerical convenience we have assumed a spherically symmetric potential $V(r) = m\omega^2 r^2/2$. The parameters are $a_{aa}/d_0 = 6 \times 10^{-3}$, $a_{bb} = 2a_{ab} = a_{aa}$, and $N = 10^5$. The dashed curve shows the squeezing obtained from the hamiltonian $H_{\mathrm{spin}} = \hbar\chi J_z^2$. The parameter χ is chosen such that the reduction of $\langle J_x \rangle$ obtained from the solution in ref. 7 is consistent with the results of ref. 11.

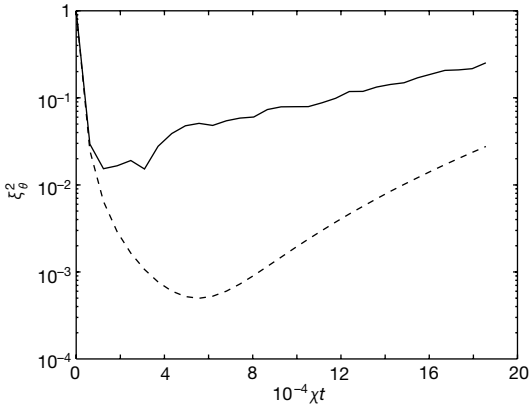

Figure 2 Quantum Monte Carlo simulation of squeezing in the presence of loss. The solid line shows squeezing obtained from the hamiltonian H_{spin} with particle loss described by a constant loss rate $\Gamma = 200\chi$. The dashed curve shows squeezing without particle loss.

the average wavefunction perform small oscillations. In the opposite case the deviations grow exponentially[11], resulting in a reduction of the overlap of the a and the b wavefunctions and a reduced squeezing. The advantages mentioned above could also be achieved with $a_{aa} \neq a_{bb}$ by using the breath-together solutions proposed in ref. 11.

Before analysing the complete system quantitatively, we estimate the amount of spin squeezing we can reach with our proposal by using a simple model. Assuming that the same wavefunction ϕ_0 for both $|a\rangle$ and $|b\rangle$ atoms is constant and independent of the number N_a, the spin-dependent part of the hamiltonian (equation (2)) may be written as $H_{\text{spin}} = \hbar\chi J_z^2$, where χ depends on the scattering lengths and the wavefunction ϕ_0. The spin squeezing produced by this hamiltonian can be calculated exactly[7]. In the limit of large N, the minimum obtainable squeezing parameter is $\xi_\theta^2 = \frac{1}{2}(3/N)^{2/3}$, which indicates that our proposal might produce a reduction of ξ^2 by a factor of $\sim N^{2/3}$; this would be more than three orders of magnitude with 10^5 atoms in the condensate.

In contrast to the simplified hamiltonian H_{spin}, the real hamiltonian (equation (2)) will also entangle the internal and motional states of the atoms; this is a source of decoherence for the spin squeezing. To quantify this effect, we have performed a direct numerical integration following the procedure developed in ref. 11. We split the whole Hilbert space into orthogonal subspaces containing a fixed number of particles N_a and $N_b = N - N_a$ in each of the internal states, respectively. In each subspace we make a Hartree–Fock variational ansatz in terms of three-dimensional spatial wavefunctions $\phi_a(N_a, t)$ and $\phi_b(N_b, t)$, which are evolved according to the time-dependent coupled Gross–Pitaevskii equations[6]. This is an approximation to the full problem which is valid in the limit of low temperatures and short times, where the population of the Bogoliubov modes[6] is small. In particular, it is a good approximation in our case with $a_{ab} < a_{aa}, a_{bb}$ where there are no demixing instabilities. With this procedure, the decoherence induced by the entanglement with the motional state is effectively taken into account. Together with the prediction from the simple hamiltonian H_{spin}, the result of the simulation is shown in Fig. 1. The two curves are roughly in agreement, confirming that the system is able to approximate the results of the hamiltonian H_{spin}. The numerical solution shows fluctuations due to the oscillations of the spatial wavefunction. The large dips at $\omega t \approx 4$, 9, 13 and 18 are the points where the atomic cloud reaches the initial width. At these instants the overlap of the wavefunctions is maximal and the two curves are very close (up to a factor of two). The small dips at $\omega t = 2$, 7, 11 and 16 correspond to the points of maximum compression. With the realistic parameters used in the figure, our simulation suggests that squeezing of three orders of magnitude is possible. Also, we note the timescale in the figure. The maximally squeezed state is reached after approximately two oscillation periods in the trap. For a fixed ratio of the scattering lengths a_{ab}/a_{aa}, the optimal time scales as $(a_{aa}/d_0)^{-2/5} N^{-1/15}$, where $d_0 = [\hbar/(m\omega)]^{1/2}$ is the width of the ground state of the harmonic potential.

The analysis so far has left out a number of possible imperfections. Specifically, we have assumed that all scattering lengths are real so that no atoms are lost from the trap, and we have not considered the role of thermal particles. To estimate the effect of particle losses, we have performed a Monte Carlo simulation[12] of the evolution of squeezing from the hamiltonian H_{spin}. The particle loss is phenomenologically taken into account by introducing a loss rate Γ which is identical for atoms in the $|a\rangle$ and the $|b\rangle$ state. In Fig. 2 we show the obtainable squeezing in the presence of loss. Approximately 10% of the atoms are lost at the time $\chi t \approx 6 \times 10^{-4}$ where the squeezing is optimal for the curve without loss. With the parameters of Fig. 1 this time corresponds to roughly two trapping periods. Such a large loss is an exaggeration of the loss compared to current experiments and the simulations indicate that even under these conditions, squeezing of nearly two orders of magnitude may be obtained. On the other hand, the effects of thermal particles can be suppressed at sufficiently low temperatures but, owing to the robustness with respect to particle losses shown in Fig. 2, we expect to obtain high squeezing even at some finite temperatures.

We believe that we have presented a simple and robust method to produce entangled states of a large number of atoms with present-day technology. These entangled states are of fundamental physical interest, and they also have possible technological applications in atomic clocks[13,14], where the projection noise $(\Delta J_\theta)^2$ is currently the main source of noise[15]. Boyer and Kasevich[14] have shown how to use an entangled state with half of the particles $N/2$ in one internal state a, and the other half in the other state b to obtain the Heisenberg limit in atomic interferometric measurements. On the other hand, it has been shown that if the atoms are prepared in a state with $\xi^2 < 1$ before they are injected into an atomic clock, it is possible to reduce the frequency noise (variance in the frequency measurements) or the measuring time to obtain a desired precision by a factor of ξ^2 compared to when the atoms are used in an uncorrelated state[13]. If the squeezing produced by our proposal was transferred into a suitable clock transition, and the atomic cloud was allowed to expand so that the role of collisions was reduced during the frequency measurement, the states could be directly applied in the current set-up of atomic clocks. Other theoretical proposals for noise reduction in systems of neutral atoms have been made[16], and a weak squeezing of the spin has recently been produced experimentally[17,18]. However, our proposal has the advantage that it offers a very strong noise reduction, and it is directly applicable to existing experimental set-ups. In future experiments that have negligible particle loss even for very long interaction times, the hamiltonian H_{spin} could also be used to produce a maximally entangled state of any number of atoms[2,19], which could reduce the frequency noise to the fundamental limit of quantum mechanics[20]. □

Methods

Here we present the derivation of equation (1) as a criterion for entanglement. An N-particle density matrix ρ is defined to be separable (non-entangled) if it can be decomposed into

$$\rho = \sum_k P_k \rho_k^{(1)} \otimes \rho_k^{(2)} \otimes \ldots \otimes \rho_k^{(N)} \tag{4}$$

where the coefficients P_k are positive real numbers fulfilling $\Sigma_k P_k = 1$, and $\rho_k^{(i)}$ is a density matrix for the ith particle. The variance of J_z may be described as $(\Delta J_z)^2 = (N/4) - \Sigma_k P_k \Sigma_i \langle j_z^{(i)} \rangle_k^2 + \Sigma_k P_k \langle J_z \rangle_k^2 - \langle J_z \rangle^2$, and using Cauchy-Schwarz's inequality and $\langle j_x^{(i)} \rangle_k^2 + \langle j_y^{(i)} \rangle_k^2 + \langle j_z^{(i)} \rangle_k^2 \leq 1/4$ we find three inequalities for separable states $\Sigma_k P_k \langle J_z \rangle_k^2 \geq \langle J_z \rangle^2$, $-\Sigma_k P_k \Sigma_i \langle j_z^{(i)} \rangle_k^2 \geq -(N/4) + \Sigma_k P_k \Sigma_i \langle j_x^{(i)} \rangle_k^2 + \langle j_y^{(i)} \rangle_k^2$, and $\langle J_x \rangle^2 \leq N \Sigma_k P_k \Sigma_i \langle j_x^{(i)} \rangle_k^2$. From these inequalities we find that any separable state obeys $\xi^2 \geq 1$ and hence any state with $\xi^2 < 1$ is non-separable.

Received 26 June; accepted 10 November 2000.

1. Special issue on quantum information. *Phys. World* **11** (2) 33–57 (1998).
2. Sackett, C. A. *et al.* Experimental entanglement of four particles. *Nature* **404,** 256–259 (2000).
3. Rauschenbeutel, A. *et al.* Step-by-step engineered multiparticle entanglement. *Science* **288,** 2024–2028 (2000).
4. Anderson, M. H., Ensher, J. R., Matthews, M. R., Wieman, C. E. & Cornell, E. A. Observation of Bose–Einstein condensation in a dilute atomic vapor. *Science* **269,** 198–201 (1995).
5. Davis, K. B. *et al.* Bose-Einstein condensation in a gas of sodium atoms. *Phys. Rev. Lett.* **75,** 3969–3973 (1995).
6. Parkins, A. S. & Walls, D. F. The physics of trapped dilute-gas Bose-Einstein condensates. *Phys. Rep.* **303,** 1–80 (1998).
7. Kitagawa, M. & Ueda, M. Squeezed spin states. *Phys. Rev. A* **47,** 5138–5143 (1993).
8. Hall, D. S., Matthews, M. R., Ensher, J. R., Wieman, C. E. & Cornell, E. A. Dynamics of component separation in a binary mixture of Bose-Einstein condensates. *Phys. Rev. Lett.* **81,** 1539–1542 (1998).
9. Stenger, J. *et al.* Spin domains in ground-state Bose–Einstein condensates. *Nature* **396,** 345–348 (1998).
10. Miesner, H.-J. *et al.* Observation of metastable states in spinor Bose-Einstein condensates. *Phys. Rev. Lett.* **82,** 2228–2231 (1999).
11. Sinatra, A. & Castin, Y. Binary mixtures of Bose-Einstein condensates: Phase dynamics and spatial dynamics. *Eur. Phys. J. D* **8,** 319–332 (2000).
12. Mølmer, K., Castin, Y. & Dalibard, J. Monte Carlo wave-function method in quantum optics. *J. Opt. Soc. Am. B* **10,** 524–538 (1993).
13. Wineland, D. J., Bollinger, J. J., Itano, W. M. & Heinzen, D. J. Squeezed atomic states and projection noise in spectroscopy. *Phys. Rev. A* **50,** 67–88 (1994).

14. Boyer, P. & Kasevich, M. A. Heisenberg-limited spectroscopy with degenerate Bose-Einstein gases. *Phys. Rev. A* **56,** R1083–R1086 (1997).
15. Santarelli, G. *et al.* Quantum projection noise in an atomic fountain: A high stability cesium frequency standard. *Phys. Rev. Lett.* **82,** 4619–4622 (1999).
16. Sørensen, A. & Mølmer, K. Spin-spin interaction and spin squeezing in an optical lattice. *Phys. Rev. Lett.* **83,** 2274–2277 (1999).
17. Hald, J., Sørensen, J. L., Schori, C. & Polzik, E. S. Spin squeezed atoms: A macroscopic entangled ensemble created by light. *Phys. Rev. Lett.* **83,** 1319–1322 (1999).
18. Kuzmich, A., Mandel, L. & Bigelow, N. P. Generation of spin squeezing via continuous quantum nondemolition measurement. *Phys. Rev. Lett.* **85,** 1594–1597 (2000).
19. Mølmer, K. & Sørensen, A. Multiparticle entanglement of hot trapped ions. *Phys. Rev. Lett.* **82,** 1835–1838 (1999).
20. Bollinger, J. J., Itano, W. M., Wineland, D. J. & Heinzen, D. J. Optimal frequency measurements with maximally correlated states. *Phys. Rev. A* **54,** 4649–4652 (1996).

Acknowledgements

This work was supported by the Austrian Science Foundation, the European Union project EQUIP, the TMR European network, the ESF under the PESC program "Quantum Information", the Institute for Quantum Information GmbH, and the Thomas B. Thriges Center for Kvanteinformatik. A.S. acknowledges the hospitality of the University of Innsbruck.

Correspondence and requests for materials should be addressed to A.S. (e-mail: anderss@ifa.au.dk).

Indium phosphide nanowires as building blocks for nanoscale electronic and optoelectronic devices

Xiangfeng Duan*†, Yu Huang*†, Yi Cui*, Jianfang Wang* & Charles M. Lieber*‡

** Department of Chemistry and Chemical Biology, ‡ Division of Engineering and Applied Sciences, Harvard University, Cambridge, Massachusetts 02138, USA*
† These authors contributed equally to this work

Nanowires and nanotubes carry charge and excitons efficiently, and are therefore potentially ideal building blocks for nanoscale electronics and optoelectronics[1,2]. Carbon nanotubes have already been exploited in devices such as field-effect[3,4] and single-electron[5,6] transistors, but the practical utility of nanotube components for building electronic circuits is limited, as it is not yet possible to selectively grow semiconducting or metallic nanotubes[7,8]. Here we report the assembly of functional nanoscale devices from indium phosphide nanowires, the electrical properties of which are controlled by selective doping. Gate-voltage-dependent transport measurements demonstrate that the nanowires can be predictably synthesized as either n- or p-type. These doped nanowires function as nanoscale field-effect transistors, and can be assembled into crossed-wire p–n junctions that exhibit rectifying behaviour. Significantly, the p–n junctions emit light strongly and are perhaps the smallest light-emitting diodes that have yet been made. Finally, we show that electric-field-directed assembly can be used to create highly integrated device arrays from nanowire building blocks.

We prepared single-crystal InP nanowires with n- and p-type doping by laser-assisted catalytic growth (LCG)[9,10]. Field-emission scanning electron microscopy (FE-SEM) images of the doped nanowires (Fig. 1a) show that the wires are up to tens of micrometres long, with diameters of the order of 10 nm. High-resolution transmission electron microscopy (TEM) images (Fig. 1a inset) show that the doped nanowires are single crystals with ⟨111⟩ growth directions. To confirm the presence and type of dopants in the nanowires, we have performed gate-dependent, two-terminal transport measurements on individual wires, as the conductance will respond in an opposite way to changes in gate voltage (V_g) for n-and p-type nanowires: $V_g > 0$ will lead to an accumulation of electrons and increase in conductance for the former, but will deplete holes and reduce conductance for the latter[11]. Figures 1b and c show the typical gate-dependent current–voltage (I–V) curves obtained from individual Te- and Zn-doped nanowires, respectively. These curves are linear or nearly linear at $V_g = 0$, indicating that the metal electrodes make ohmic contact to the nanowires. This ohmic nature was substantiated by conductance and four-terminal measurements (see Supplementary Information). The transport data recorded on Te-doped nanowires (Fig. 1b) show an increase in conductance for $V_g > 0$, while the conductance decreases for $V_g < 0$. These data clearly show that Te-doped InP nanowires are n-type. Gate-dependent transport data recorded on Zn-doped nanowires show

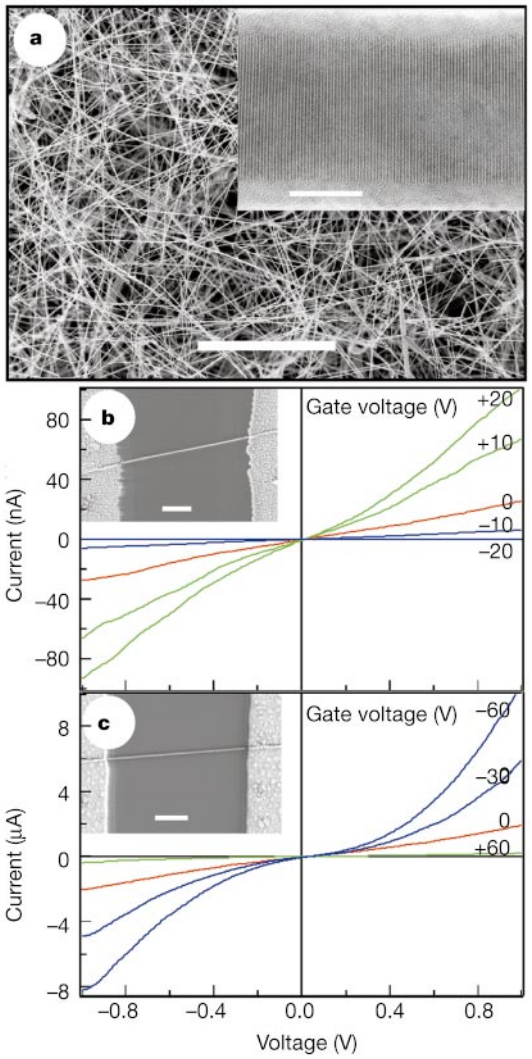

Figure 1 Doping and electrical transport of InP nanowires. **a**, A typical FE-SEM image of Zn-doped InP nanowires. Scale bar, 10 μm. Inset, lattice resolved TEM image of one 26-nm-diameter NW. The (111) lattice planes are visible perpendicular to the wire axis. Scale bar, 10 nm. The TEM studies show that nanowires are typically coated with a 1–2-nm amorphous overlayer. This thin layer is attributed to oxides formed when the nanowires are exposed to air after synthesis. The overall composition of individual nanowires determined by energy dispersive X-ray analysis was found to be 1:1 In:P, thus confirming their stoichiometric composition. **b** and **c**, Gate-dependent I–V behaviour for Te- and Zn-doped NWs, respectively. Insets show the nanowire measured with two-terminal Ni/In/Au contact electrodes. Scale bars, 1 μm. The diameter of the nanowire in **b** is 47 nm, while that in **c** is 45 nm. Gate voltages used in the measurements are indicated on the corresponding I–V curves (right side). Data were recorded at room temperature.